Title

In vitro and in vivo metabolism of N-adamantyl substituted urea-based soluble epoxide hydrolase inhibitors

Authors

Liu, Jun-Yan

Tsai, Hsing-Ju

Morisseau, Christophe

et al.

Peer reviewed

HHS Public Access
Author manuscript

Biochem Pharmacol. Author manuscript; available in PMC 2016 December 15.

In vitro and *in vivo* metabolism of *N*-adamantyl substituted urea-based soluble epoxide hydrolase inhibitors

Jun-Yan Liu[a,b,†], **Hsing-Ju Tsai**[b,†], **Christophe Morisseau**[b], **Jozsef Lango**[b], **Sung Hee Hwang**[b], **Takaho Watanabe**[b], **In-Hae Kim**[b], and **Bruce D. Hammock**[b,*]

Bruce D. Hammock: bdhammock@ucdavis.edu

[a]Center for Nephrology and Clinical Metabolomics, Division of Nephrology and Rheumatology, Shanghai Tenth People's Hospital, Tongji University School of Medicine, Shanghai, 210072, P. R. China

[b]Department of Entomology and Nematology, and UC Davis Comprehensive Cancer Center, University of California, Davis, CA 95616, USA

Abstract

N,N′-Disubstituted urea-based soluble epoxide hydrolase (sEH) inhibitors are promising therapeutics for hypertension, inflammation, and pain in multiple animal models. The drug absorption and pharmacological efficacy of these inhibitors have been reported extensively. However, the drug metabolism of these inhibitors is not well described. Here we reported the metabolic profile and associated biochemical studies of an *N*-adamantyl urea-based sEH inhibitor 1-adamantan-1-yl-3-(5-(2-(2-ethoxyethoxy)ethoxy)pentyl)urea (AEPU) *in vitro* and *in vivo*. The metabolites of AEPU were identified by interpretation of liquid chromatography-mass chromatography (LC-MS), liquid chromatography-tandem mass spectrometry (LC-MS/MS) and/or NMR. *In vitro*, AEPU had three major positions for phase I metabolism including oxidations on the adamantyl moiety, urea nitrogen atoms, and cleavage of the polyethylene glycol chain. In a rodent model, the metabolites from the hydroxylation on the adamantyl group and nitrogen atom were existed in blood while the metabolites from cleavage of polyethylene glycol chain were not found in urine. The major metabolite found in rodent urine was 3-(3-adamantyl-ureido)-propanoic acid, a presumably from cleavage and oxidation of the polyethylene glycol moiety. All the metabolites found were active but less potent than AEPU at inhibiting human sEH. Furthermore, cytochrome P450 (CYP) 3A4 was found to be a major enzyme mediating AEPU metabolism. In conclusion, the metabolism of AEPU resulted from oxidation by CYP could be shared with other *N*-adamantyl-urea-based compounds. These findings suggest possible therapeutic roles for AEPU and new strategies for drug design in this series of possible drugs.

*Corresponding author: Tel.: +1 530 752 751, Fax: +1 530 752 1537.
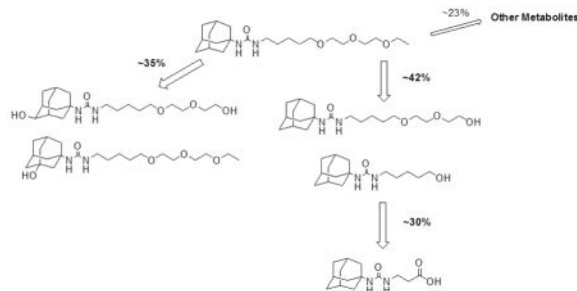†These authors contributed equally to this work.

Conflict of interest statement

Graphical Abstract

Keywords

soluble epoxide hydrolase; drug metabolism; LC-MS/MS; NMR; cytochrome P450s

1. Introduction

The mammalian soluble epoxide hydrolase (sEH; EC 3.3.2.10) is involved in mediating the metabolism of the endogenous lipids epoxides such as epoxyeicosatrienoic acids (EETs) that are derived from arachidonic acid. The sEH converts epoxide-containing substrates into the corresponding more polar and less potent vicinal diols [1, 2]. EETs are vasodilation mediators through the activation of the Ca^{2+}-activated K^+ channels in endothelial cells [3] which benefit many renal and cardiovascular diseases [4]. EETs are reported to be involved in the cell angiogenesis and proliferation [5, 6] which may offer a protective role in ischemic and reperfusion injury. Furthermore, the EETs are anti-inflammatory mediators in endothelial cells by inhibiting the expression of the proatherogenic mediator vascular cell adhesion molecule-1 that is induced by tumor necrosis factor-α (TNF-α) [7]. In addition, EETs suppress the NF-κB-mediated expression of cytokines by activating PPARγ [8]. Thus, the inhibition of sEH by using potent and reversible sEH inhibitors leading to the accumulation of EETs has been demonstrated an effective approach for treating several diseases including hypertension [9], inflammation [10, 11], cardiac hypertrophy [12], and ischemic stroke [13], pain [14–17], and ischemic myocardial infarction [18] in multiple animal models [19]. Evidence is building that reduction of endoplasmic reticulum stress is a common underling mechanism for many of these therapeutic effects [20–25].

Among the thousands of sEH inhibitors that developed by this and other laboratories, *N,N′*-Disubstituted urea-based chemicals, such as 12-(3-adamantyl-ureido)-dodecanoic acid (AUDA), 1-adamantan-3-(5-(2-(2-ethylethoxy)ethoxy)pentyl) urea (AEPU), 1-(1-acetypiperidin-4-yl)-3-adamantanylurea (APAU), *trans*-4-[4-(3-adamantan-1-ylureido)-cyclohexyloxy]-benzoic acid (*t*-AUCB), and 1-(4-trifluoro-methoxy-phenyl)-3-(1-propionylpiperidin-4-yl)urea (TPPU) are the most commonly reported sEH inhibitors [19, 26]. These inhibitors tightly bind to the sEH enzyme with the K_Is in the nanomolar to picomolar range often with high target occupancy [27–30]. The pharmacological effects of *N*-adamantyl-urea-based sEH inhibitors have been investigated extensively in various animal disease models [9–18]. And some sEH inhibitors have been moved to clinical trials (NCT00654966, NCT01762774, NCT02006537 and NCT02262689). In addition, the

pharmacokinetics (PK) profiles of sEH inhibitors with the focus on the time course of drug blood levels in murine, rodent, canine, equine, and primate models were reported previously [31–35]. However, as an important part during the process of drug development, drug metabolism of *N*-adamantyl-urea-based sEH inhibitors has not been reported while only one cyclohexyl-urea-based sEH inhibitor, 1-cyclohexyl-3-dodecyl-urea (CDU), was reported previously with regard to its metabolism *in vitro* [36]. Here we report the *in vitro* and *in vivo* drug metabolism characteristics and associated metabolism mechanisms of *N*-adamantyl-urea-based sEH inhibitors.

2. Materials and Methods

2.1. Animals and Chemicals

All the animal experiments were conducted following the protocols approved by the Animal Use and Care Committee of University of California-Davis. Male rats (Sprague Dawley, 10–12 weeks) and male mice (C57BL/6, 8 weeks) were purchased from the Charles River Laboratories (CA). Cytochrome P450s (CYPs), rat and human liver S9 fraction were purchased from BD Biosciences (Franklin Lakes, NJ). 1-(5-Butoxypentyl)-3-adamantylurea (surrogate), 1-adamantanyl-3-decylurea (ADU, internal standard), AEPU and *t*-AUCB, were synthesized in this laboratory by using the methods previously published [27, 30, 37]. β-Nicotinamide adenine dinucleotide phosphate sodium salt (NADP+), glucose-6-phosphate dehydrogenase (G6PDH), D-glucose-6-phosphate monosodium salt (G6P), anhydrous magnesium chloride ($MgCl_2$), sodium chloride (NaCl), ketoconazole, Chromium trioxide, sulfuric acid, and formic acid (98 %) were obtained from Sigma (St. Louis, MO). HPLC-grade methanol, acetonitrile, ethyl acetate, reagent-grade monobasic monohydrate sodium phosphate and anhydrous dibasic sodium phosphate were purchased from Fisher Scientific (Pittsburgh, PA). Water (>18.0 MΩ) used was purified by NANO pure II system (Barnstead, Newton, MA).

2.2. *In vitro* incubation

AEPU (1 mmol in 10 μl DMSO) was incubated with 890 μl of human or rat liver S9 fraction at protein concentration of 2.5 mg/ml in a 20 ml glass vial. The solution was pre-incubated for 5 minutes in a shaking bath at 37 °C as previous described [38]. The reaction was initiated by adding 100 μl of NADPH generating system (NADP+ (2 mM), glucose 6-phosphate (57 mM), glucose 6-phosphate dehydrogenase (3.5 units), and magnesium chloride (50 mM) dissolved in 100 mM sodium phosphate buffer (pH 7.4) and terminated after 2 h reaction by adding 4 ml of cold ethanol. After vigorous mixing for 30 sec, the mixture was centrifuged at 2862×g for 5 min. The supernatant was divided equally into two tubes, one for fluorescent activity assay and another for the liquid chromatography-coupled tandem mass spectrometry (LC-MS/MS) and liquid chromatography-mass chromatography (LC-MS) analyses.

2.3. *In vivo* metabolism study

Pathogen-free male rats (Sprague Dawley, 10–12 weeks, 250–350 g, N = 4) were housed in temperature-controlled rooms with 12 h of light per day. The animals were fed a standard rodent chow and permitted full access to food and water prior to experiments. Rats were

orally treated with 10 mg/kg of AEPU in oleic rich triglycerides and housed in a metabolic chamber with sufficient food and water for 24 hours. The urine samples were collected before and 24 h after the drug treatment, respectively. In a polypropylene glycol tubes, surrogate solution (20 μl) and ethyl acetate (1mL) were added to urine (1 ml). After vigorous mixing for 30 sec, the mixture was centrifuged at $11,000 \times g$ for 5 min. The organic layer was transferred into a clean glass tube (4 mL). Another 1 ml of ethyl acetate was added for the second extraction. The organic layers were combined and dried under a nitrogen atmosphere and the residues were reconstituted in 100 μl of methanol. Aliquots (5 μl) of the reconstituted samples were analyzed by LC-MS/MS.

Pathogen-free male mice (C57BL/6, 8 weeks, 22–25 g, N = 4) were used for the metabolism study of *t*-AUCB according to the procedure mentioned above. Specifically, after centrifugation at $11,000 \times g$ for 5 min, the collected urine (200 uL) was transferred into a clean eppendorf tube (1.5 mL) containing 600 mL of the internal standard solution (200 nmol/L ADU in acetonitrile). After strong mixing on a Vortex mixer for 5 min, the mixture was centrifuged at $11,000 \times g$ for 5 min and then the supernatant (50 uL) was transferred into a 150 glass insert kept in a 4 mL vial for LC-MS/MS analysis.

2.4. LC-MS/MS analysis

The samples prepared were analyzed using a Micromass Quattro Premier triple quadrupole tandem mass spectrometer (Micromass, Manchester, UK) equipped with Ultra Performance LC (UPLC; Waters Corporation, Milford, MA). The metabolites was separated with an Acquity column (BEH C18, 100×2.1 mm I. D., 1.7 μm; Waters Corporation) at a flow rate of 0.3 ml/min at 40 °C. Solvent A was a mixture of water/acetonitrile (9/1, v/v) containing 0.1 % of formic acid and solvent B was acetonitrile containing 0.1 % of formic acid, respectively. Mobile phases were mixed with a linear gradient from 10 % B to 60 % B over 30 min, 60% B to 100% B for 5 min, and then isocratic for 5 min with 100 % B. The post run was carried out to equilibrate the column to the initial conditions for 2 min before next run. Aliquots of 5 μl of standard and prepared samples were injected for the separation on the column. The ESI was performed in the positive ion mode with a capillary voltage at 1 kV. The source and the desolvation temperature were set at 125 °C and 300 °C, respectively. Cone gas (N_2) and desolvation gas (N_2) were maintained at flow rates of 50 and 650 l/h, respectively. Mass spectra of the precursor ions were obtained while scanning over the range of 50 to 500 m/z at 1 s/scan. Data were acquired in the continuum mode. Ultra pure argon was used as a collision gas at a pressure of 2.5 mTorr for collision-induced dissociation (CID), which was performed for each selected metabolite after full scan to provide the information of key fragments of target metabolites. The *m/z* of precursors and key fragments of APEU and its metabolite were summarized in Table 1. Data were evaluated with MassLynx software (Ver. 4.1).

2.5. Recombinant human CYPs incubation

To investigate the CYPs activity on AEPU, a final concentration of 1 μM of AEPU and 20 pmol/ml of various CYPs were pre-incubated in 178 μl of 100 mM of sodium phosphate buffer (pH 7.4) for 5 min at 37 °C. The reaction was initiated by adding 20 μl of NADPH generating system and incubated for 0 and 30 min. The reaction was stopped by adding 800

μl of internal standard solution (200 nM ADU in methanol). Then, the mixtures were processed as described previously in *2.2*. The aliquot (5 μl) was then analyzed as described in *2.4*. To investigate the role of CYP 3A4 in AEPU, 10 uM of ketoconazole (KTZ), a selective CYP 3A4 inhibitor, was added to 178 μl of human liver microsomes (0.056 mg/ml). After pre-incubation for 5 minutes, the reaction was initiated by adding a NADPH generating system. Samples were incubated for 30 min at 37°C as previously described, followed by protein precipitation and LC-MS/MS analysis as described above.

2.6. Enzymatic preparation of AEPU metabolites

The rat liver S9 fraction was prepared as described previously [36] and the protein concentration was determined by the Bradford protein assay (Bio-rad laboratories, Hercules, CA). AEPU (75 mg) was dissolved in methanol (4 ml) to form a clear solution. AEPU solution was transferred into a clean flask with 336 ml of phosphate buffer (100 mM, pH 7.4) and the mixture was shaken slowly until it was clear. Rat liver S9 fraction (20 ml) was added to a final concentration of 1 mg protein/ml. After pre-incubation at 37°C for 5 min, a NADPH generating system (40 ml) was added as described above and then incubated for 4 hours. To stop the enzymatic reaction, ethyl acetate (400 ml) was added and the mixture was vigorously shaken. To precipitate protein, sodium chloride was added to saturation and the solution was held at 37°C for two hours. After forming a clear two layer solution, the upper organic layer was collected. The extraction of water layer was repeated three times. The upper organic layers were combined and dried under a blanket of nitrogen gas. The dried products were reconstituted with 2 ml of methanol followed by repeated filtration over a column filled with Sephadex LH-20 (GE health care, Pittsburgh, PA) washed by methanol. The collected fractionations (1 mL each) were analyzed by LC-MS. If the fractionations contained more than one compound, further separation was performed with HyperSep C18 column (Thermo Fisher scientific, Waltham, MA) equilibrated with 2 volume of water containing 60% methanol. After loading samples, the columns were washed with 5 ml of 60% methanol in water and then 15 ml of 70% methanol in water followed by 5 ml of 80%, 90%, and 100% methanol in water, respectively. Each 1 ml of eluent was collected and analyzed by LC-MS. The fractionations with single compound were used to identify the chemical structure by NMR and to determine the inhibitory activity by the fluorescent assay.

2.7. NMR analysis

AEPU and its metabolites were dissolved in $CDCl_3$ for NMR data collection. All NMR data were collected on a Bruker Avance 500 spectrometer with ^1H observed at 500 MHz. The chemical shifts were expressed in δ (ppm) relative to SiMe4 (the internal standard) with coupling constants *J* expressed in Hz.

2.8. sEH activity assay

IC_{50} values were determined by using fluorescent assay according to the previously reported protocol [39].

3. Results

3.1. *In vitro* metabolites of AEPU

To investigate the metabolites of AEPU, the extracted supernatant from the incubation of AEPU with rat and human liver S9 fractions was monitored by LC-MS with a full scan mode (Fig. 1.). As expected, the major metabolites obtained from liver S9 fraction incubation are hydroxylated products. According to the retention time of the synthetic standards, the chromatogram can be divided into three parts including "additional" polar metabolites (2.5–6 min), adamantyl hydroxylation metabolites (6–12 min) and polyethylene glycol chain cleavage metabolites (12–18 min). The relative amounts of AEPU's polar metabolites differ between rat and human liver S9. In addition for both species, additional polar metabolites (2.5–6 min) were detected but in very low relative amount compared to the less polar metabolites. Therefore, the tentative structures of these minor metabolites are not discussed in this paper. M1 to M6 are probably the metabolites with hydroxylation on the adamantyl group because the retention time is close to a synthetic standard with β-hydroxylation on the adamantyl group (M2)[40]. M7 to M14 are likely the metabolites with hydroxylation on the polyethylene glycol chain because their retention times are close to the synthetic standard with ω-hydroxylation at the end of polyethylene glycol chain (M7)[37]. These tentatively assigned structures were also supported by the precursor and key fragments of the metabolites that are detailed below in *3.3*.

3.2. *In vivo* metabolites of AEPU

To investigate the *in vivo* metabolism of AEPU in a rodent model, rat urine was collected in the metabolic chamber before and 24 hr post drug treatment, respectively. The collected urine was prepared for the examination by LC-MS with the full scan mode (Fig. 2.). The metabolites with hydroxylation on the adamantyl group and nitrogen (M1 to M6) are present, suggesting that these metabolites resist further oxidation or conjugation *in vivo*. The metabolites with hydroxylation on the glycol chain were observed near or under the limit of detection probably due to rapid oxidation of the primary alcohols, and excretion and/or conjugation of those metabolites. The remaining metabolites shown on the chromatogram are acid metabolites including M8 and M11. However, there is one other major metabolite, M15, found in the urine samples. In addition, more polar metabolites were observed in *in vivo* metabolism, indicating the involvement of multiple metabolic pathways resulting in a more complicated metabolic pattern *in vivo*.

3.3. The structural identification of *in vitro* metabolites of AEPU by LC-MS and LC-MS/MS

An understanding of the generation and conversion mechanisms of the three key fragments of AEPU by the collision-induced dissociation (CID) spectrum is critical for establishing the structures of its metabolites (Table 1). Fragment **1** (*m/z* 135) resulted from the cleavage between *N*-adamantyl and urea groups while fragment **2** (*m/z* 152) and fragment **3** (*m/z* 220) were formed through a proton shift from nitrogens on the urea group (Table 1.). Fragments **1** and **2** are the characteristic products of adamantyl substituted urea sEH inhibitors, which has been demonstrated by previous studies [31, 41].

The structures of the key metabolites AEPU are summarized in Table 1. The metabolites M1, M2 and M6 afford the same protonated molecular peak at *m/z* 413, indicating that these metabolites are the mono-hydroxylation products of AEPU (*m/z* 397). M1, M2 and M6 have the same product ion with the *m/z* at 220 showing that the subunit yielding fragment **3** is untouched during the formations of M1, M2 and M6. Furthermore, the product ions of *m/z* 151 and 168 replaced the fragments **1** and **2** of AEPU at *m/z* 135 and 152 respectively, which suggests that fragment **1** (adamantyl moiety) is hydroxylated during the biosyntheses of M1, M2 and M6. M5 affords the protonated molecular peak at *m/z* 411 with product ions at *m/z* 220 indicating the hydroxylated fragment **1** rearranges to a ketone moiety. These metabolite identifications were further supported with chromic acid oxidation on a micro scale (Fig. 3). After chromic acid oxidation, M1 and M6 disappear and M5 increase indicating that M1 and M6 are secondary hydroxylation metabolites oxidized to ketone product (M5). And because M1 and M6 formed the same product M5 by chromic acid oxidation, M1 and M6 should be stereoisomers. In addition, the retention time pattern for M1 and M2 were similar to that of the two synthetic metabolite reference standards of another *N*-adamantyl-urea-based sEH inhibitor, 1-(1-acetypiperidin-4-yl)-3-adamantanylurea (APAU), showing that the M1 similar metabolite was eluted earlier than the M2 similar metabolite in the same chromatographic column. Therefore, M6 is tentatively identified as the structure as shown in Table 1. Because M2 is stable to chromic acid oxidation, it is identified as a tertiary hydroxylation product on the adamantyl moiety. Furthermore, M2 was established as a tertiary hydroxylation product (Table 1) for its retention time and CID product ion spectra identical to those of the synthetic standard.

The metabolites M3 and M4 afforded the same protonated molecular peak at *m/z* 413 that is diagnostic of the mono-hydroxylation products (Table 1). However, they contain product ions with the *m/z* at 135 for fragment **1** (adamantyl moiety) and 220 for fragment **3** indicating the hydroxylation occurs on one of the urea nitrogens. After chromic acid oxidation M3 and M4 are stable, supporting the hydroxylation on the nitrogen groups (Fig. 3). Assuming that the ionization efficiencies on mass of these metabolites are similar, the amounts of M3 and M4 are much smaller than M2.

The metabolites M7 (*m/z* 281), M9 (*m/z* 325), and M10 (*m/z* 369) had the protonated molecular peaks from AEPU (*m/z* 397), indicating the cleavage of the polyethylene glycol chain (Table 1). These were supported by the same key fragments **1** (*m/z* 135) and **2** (*m/z* 152) as those of AEPU. The cleavage fragments were also found at *m/z* 192 for M10, *m/z* 148 for M9, and *m/z* 104 for M7, respectively, probably through the similar mechanism as for fragment **3**. In addition, the retention time and CID product ion spectra of M7 are identical to those of the synthetic standard [37]. The corresponding acids were also determined as M8 (*m/z* 295), M11 (*m/z* 339), and M12 (*m/z* 383). M13 and M14 afford the same protonated molecular peaks at *m/z* 413, indicating that these metabolites are the hydroxylation products of AEPU. M13 and M14 have the same product ions with the *m/z* at 135 and 152 showing that they have the subunit critical to produce the same fragment **1** and **2** as AEPU and the hydroxylation occurs on the polyethylene glycol chain. M13 was identified to with the structure as Table 1 for its retention time and mass data identical to those of the synthetic standard. Furthermore, after chromic acid oxidation, the metabolites of

the polyethylene glycol chain (M7, M9, and M10) which are primary hydroxylation were further oxidized to corresponding acids (M8, M11, and M12) (Fig. 3).

M15 is a propanoic acid metabolite indicated by the fragment ion at *m/z* 90. The key fragment ion of M15 was *m/z* 135, indicating it is derived from the AEPU fragment retaining the adamantyl group. Furthermore, the chromatogram shows more polar metabolites in the urine samples, indicating there is further metabolism of the tentatively identified AEPU products. We also monitored the murine whole blood samples from previous study for comparison [40]. AEPU is metabolized rapidly *in vivo* and multiple metabolites were observed after 30 minutes (Fig. 4). It could be observed that metabolites with hydroxylation on the adamantyl group and nitrogen (M1–4 & M6) were detected in the blood for 8 hours. This suggests that hydroxylated metabolites of adamantane are formed rapidly and seem to resist further oxidation and conjugation probably due to steric hindrance. On the other hand, most metabolites with hydroxylation on the polyethylene glycol chain are further oxidized. Only two acid products, M8, and M15, were detected in the blood samples. Probably their half-lives are short since they were under the detection limitation in blood 6 hours post administration. The other acid metabolite detected in rat urine, M11, was under detection limit in mouse whole blood.

3.4. The structural identification of key *in vitro* metabolites of AEPU by NMR

The structures of M1 and M2 are also supported by those unchanged signals of polyethylene glycol between δ 3.1 and 3.7 in ^{1}H-NMR spectra when compared to that of AEPU (Table 2 and Fig. 5). No additional peak appears between δ 3.0 and 4.5 in the ^{1}H NMR spectrum of M2 when compared with that of AEPU, which requires that the hydroxylation have to occur at C-2 (or its equivalent C-2′ or C-2″) during the production of M2. This is supported substantially by the following changes to the adamantyl including 1) the original broad singlet at δ 2.09 (br s, 3H, H-2, H-2′ and H-2″) in AEPU′s spectrum was replaced by a new broad singlet at δ 2.24 (br s, 2H, H-2′ and H-2″) in M2; 2) the broad singlet at δ 1.97 (br s, 6 H, 2H-3, 2H-3′ and 2H-3″) in AEPU′s ^{1}H-NMR spectrum was replaced by the broad singlet at δ 1.94 (br s, 2H, H-3) and the broad singlet at δ 1.84 (br s, 4H, H-3′ and H-3″) in M2′s ^{1}H-NMR spectrum, respectively; and 3) the broad singlet at δ 1.67 (br s, 6H, H-1, H-1′ and H-1″) in AEPU′s ^{1}H-NMR spectrum is replaced by the broad singlet at δ1.67 (br s, 4 H, H-1 and H-1′) and the multiplet at δ 1.48 (m, 2H, H-1″) in M2′s ^{1}H-NMR spectrum, respectively. In addition, the synthetic standard afforded the identical ^{1}H-NMR and MS spectra to M2. An additional broad singlet appears at δ 3.94 (br s, 1H) in the ^{1}H NMR spectrum of M1 when compared with those of AEPU and M2, indicating that C-1 (or its equivalent C-1′ or C-1″) may be hydroxylated [42]. However, the signals between δ 2.2 and 1.5 overlapped heavily which makes it difficult to unambiguously assign the corresponding signal shifts of the rest protons in the adamantyl moiety due to the hydroxylation of C-1. Nevertheless, the pattern of retention time for M1 and M2 was similar to those of the synthetic standards of the M1- and M2-like metabolites of APAU, supporting the assigned structure for M1.

On the other hand, M7 and M10 have similar signals between δ 1.5 and 2.1 for the adamantyl moiety to those of AEPU indicating the hydroxylation occurs on the polyethylene

glycol chain. M7 affords only 5 methene signals at δ 3.63 (t, 6.4, 2H, H-12), 3.11 (dd, 10.6, 6.5, 2H, H-8), 1.57 (m, 2H, H-11), 1.49 (m, 2H, H-9) and 1.39 (m, 2H, H-10), respectively, indicating that a hydrolysis occurred between O-13 and C-14 resulting in the formation of M-7. The ethyl signals for AEPU at δ 3.53 (q, 7.0, 2H, H-20) and 1.21 (t, 7.0, 3H, H-21) missing in the ^{1}H-NMR spectrum of M10 indicates that the hydrolysis between O-19 and C-20, resulting in the downfield shift of the two methenes (C-18 and C-17) to δ 3.73 (br t, 5.0, 2H, H-18) and 3.62 (br t. 5.0, 3H, H-17), respectively.

3.5. CYP 3A4 is the major CYP mediating the metabolism of AEPU

Because the hydroxylated metabolites are known to occur through CYPs, six commercially available CYPs (CYP1A1, CYP2B6, CYP2D6, CYP2C9, CYP3A4, and CYP4F11) were tested on the metabolism of AEPU (Fig. 6A). CYP3A4 is the major enzyme while CYP2D6 is minor enzyme involved in the *in vitro* metabolism of AEPU. M2, M7 and M10 are three major metabolites found after incubation and no acid metabolites have been determined. In addition, based on the response area, it is clear that still other adamantyl metabolites are produced. When using ketoconazole, a selective inhibitor of CYP 3A4, the metabolism of AEPU in human liver S9 fraction ceased (Fig. 6B). This inhibitory selectivity of ketoconazole indicates that CYP 3A4 is a major enzyme mediating the metabolism of AEPU.

3.6. The potencies of metabolites

Using small amount of the AEPU metabolite mixture, it was found that metabolites of AEPU from rat and human liver S9 fraction also have sEH inhibitory activity (Fig. 7). Specifically, after removal of the remaining AEPU at 30 and 60 min, the metabolite mixture also had inhibitory ability against respective sEH enzymes although the inhibitory action was weaker than AEPU. In addition, the AEPU metabolite mixture was separated into fractions for potency determination with the fluorescent assay (Fig. 8), showing the potency for some fractions. The AEPU metabolites produced in the rat liver S9 fraction for NMR analysis were evaluated for potency with the fluorescent assay for sEH inhibition (Table 3). M1 and M2 identified as hydroxylation products on the adamantyl moiety have weaker potencies (30–100 fold lower) compared to AEPU. On the other hand, metabolites with hydroxylations on the polyethylene glycol chain (M7 and M10) are more potent than M1 and M2 but similar potent to AEPU. Moreover, it was observed that the potencies decrease when the polyethylene glycol chain is shortened.

4. Discussion

Drug metabolism study plays a vital role in the process of drug development because it provides comprehensive understanding of the alterations of drugs within the body mediated by a vast array of enzymes. So far, *in vitro* metabolism has been described for only 1-cyclohexyl-3-dodecyl-urea (CDU) [36]. However, metabolism of *N*-adamantyl substituted urea-based sEH inhibitors has been occasionally reported *in vivo* whereas their pharmacological effects and pharmacokinetics profiles have been reported extensively [11, 27, 32, 40, 43–46]. Therefore, here we report the *in vitro* and *in vivo* metabolism of *N*-adamantyl substituted urea-based sEH inhibitors.

To overcome the limitation such as poor water solubility and high melting point in early sEH inhibitors like CDU, AEPU is composed with an adamantyl moiety to increase potency on the target enzyme and a polyethylene glycol chain to increase water solubility and lower melting point which facilitate formulation to increase oral bioavailability. AEPU is a potent sEH inhibitor *in vitro* and effective on several animal models [12, 40]. However, the blood level of AEPU was undetectable in those animals through the whole time course. It was hypothesized that the biological effects may due in part, to the metabolites of AEPU collectively in addition to low levels of AEPU bound to the target enzyme [40]. In other words, AEPU is also an excellent compound to investigate the metabolism of *N*-adamantyl substituted urea-based sEH inhibitors. The insights into the route of AEPU metabolism can help in the refinement of more stable inhibitors for future *in vivo* applications. This was supported by the later findings that conformationally restricted *N,N′*-disubstituted urea-based compounds, like *t*-AUCB and TPPU, result in more stable *in vivo* and higher blood levels than AEPU [31, 34].

In this study, we firstly determined the structures and the inhibitory activities of major AEPU metabolites mediated by the liver subcellular fractions based on two facts below: 1) Liver subcellular fractions are convenient and inexpensive models to predict the drug metabolism *in vivo* [47, 48]; 2) The liver S9 fractions contain both phase I and phase II enzymes for understanding entire AEPU metabolism. As expected, we observed that the metabolism of AEPU was greater in liver S9 fractions than that in liver microsomal preparations, indicating that some cytosol enzymes in liver S9 fraction also contributed to AEPU metabolism (Fig. 7).

The metabolism of AEPU mainly occurred in two parts (Fig. 9): a hydroxylation on the adamantyl group (30%; M1, M2 and M6) and an oxidation on the polyethylene glycol chain (42%; M7, M9, M10, M13, and M14). M1, M2, and M6 are stable hydroxylation metabolites on the adamantyl moiety in *vivo* that were also observed in blood (Fig. 4.) and urine (Fig. 2.). Like other adamantyl derivatives, it is expected that further conjugation such as glucuronidation may occur on those hydroxylation metabolites *in vivo* but steric hindrance will likely result in slow conjugation [42, 49]. Relatively small amounts of the secondary hydroxylation products (M1 and M6) can be further metabolized to a secondary ketone (M5). This may be mediated by alcohol dehydrogenase in cytosol, a generally known enzyme that catalyzes secondary alcohols to the formation of corresponding ketones. The inhibitory activities of M1 and M2 are 30–100 fold lower than AEPU (Table 2) and it is expected that M6 is also less potent than AEPU. However, because they are relatively stable resulting in high steady state blood concentrations *in vivo* [40], it is most likely that those metabolites contribute to the pharmacological effects of AEPU collectively.

The second pathway is oxidation of the polyethylene glycol chain of AEPU. While most metabolites of this oxidation were hydroxylated compounds after *in vitro* incubation (M7, M9, M10, M13, and M14), more acid metabolites were found *in vivo* (M8, M11, and M12). Because M8 is one of major metabolites in plasma, it is expected that further oxidation occurs on these metabolites to form M8 *in vivo*. M15 was found in both plasma and urine, suggesting that M15 is the final metabolite derived from M8 by β-oxidation. Due to the lack of the authentic standard, the exact amount of hydroxylation metabolites was not analyzed

quantitatively. However, the pharmacological effects may derive from some of these metabolites collectively. For example, M10 is similar potent to AEPU on the human sEH enzyme due to the long polyethylene glycol chain (Table 2). When the glycol chain was shortened to M7, the inhibitory potency decreased 6 fold compared to M10 and AEPU. One can expect that major metabolite in plasma, M8, has similar or lower potency to M7. These results are similar to the previous study [30] that the inhibitory potencies decreased while the alkyl chain was shortened. It was determined that the inhibitory potency of 4-(3-adamantan-1-yl-ureido)butanoic acid which is similar to M15 is very weak. One can expect that the major metabolite in urine, M15, has very low or negligible biological effect *in vivo*. Thus, some of the pharmacological effects of AEPU may result from the metabolites with hydroxylation on the polyethylene glycol chain but these effects will be of short duration because of their metabolic instability due to rapid oxidation and conjugation.

In addition, there are 23% of AEPU metabolized to other products. M3 and M4 represent oxidation on the nitrogen of the urea functional group. Though the amount is relatively small, M3 and M4 are also stable in blood and urine. M3 and M4 are unlikely to be potent sEH inhibitors because the hydroxylation blocks the active binding site of urea functional group [50]. Furthermore, the concentration of M3 and M4 are too low to result in pharmacological effects even though they are also stable *in vivo*. Furthermore, more polar metabolites of AEPU were observed in the rat urine (Fig. 2). It is hard to determine the structures of those metabolites due to low amount and the lack of specific fragments that can be traced to AEPU. However, by the mass spectrum, some of them are suggested as metabolites with two hydroxylations on AEPU. Because of the high polarity, one can expect low potencies from these metabolites on the sEH [51].

When AEPU was incubated *in vitro* without NADPH, it failed to generate metabolites indicating that the metabolism is mainly catalyzed by CYPs. To determine the major metabolizing enzyme, six CYPs were used in the study. Among them, five of the CYPs we used belonging to CYP enzyme families 1–3 which are responsible for 70–80% of phase I-dependent drug metabolisms. The major CYP to metabolize AEPU is CYP3A4 which forms most adamantyl oxidation metabolites and the minor one is CYP2D6 which forms most M10 with chain cleavage of polyethylene glycol chain. It was also supported by the fact that AEPU is metabolized slowest in the canine liver microsomes and S9 fraction because dogs have very low activity of CYP3A4 compared to other species [52]. In addition, with the ketoconazole, a selective CYP3A4 inhibitor, the *in vitro* metabolism of AEPU was dramatically reduced, which cautions use AEPU-like sEH inhibitors clinically with grapefruit juice or other CYP3A4 inhibitors. Other compounds with adamantyl moieties are metabolized by CYP2C19 and CYP2D6 [53] indicating activities of CYPs are complementary and overlapping. Besides the CYPs, the metabolites with N-oxidation may be involved with flavin-containing monooxygenase which need further experiments.

Among the metabolic pathways of AEPU (Fig. 9), oxidation on the adamantyl moiety and nitrogen atoms could be shared by other adamantyl substituted urea based sEH inhibitors. This was supported by a separate metabolism study of another potent sEH inhibitor, *t*-AUCB, in a murine model. In the mouse, urine collected one day after administration of *t*-AUCB (1 mg/kg, p.o.), five metabolites could be detected as the structures in Fig. 10 based

on the quasimolecular mass and associated key fragments, as well as the retention time pattern compared with those of the metabolites of AEPU. In contrast, the metabolism occurred at cyclohexyloxy-benzoic acid was much lower than those on adamantyl moiety. This supported our hypothesis that conformationally restricted *N,N′*-disubstituted compounds could improve their bioavailability, which was also supported by the higher blood levels of those inhibitors monitored in pharmacokinetic studies [31, 32].

It should be noted that the liver microsome and S-9 fraction from different species like mouse, rat, dog, and human resulted in different effects on *in vitro* metabolism of AEPU (Fig. 7). When compared to other species tested, dog liver microsome is likely less active than those from mouse, rat, and human on AEPU metabolism, resulting in the higher level of AEPU remaining in the metabolic mixture (Fig. 7A). However, only slight difference was observed among mouse, rat, and human liver microsome. When the in vitro metabolism mediated by liver S9 fractions, the order of activity looks like dog < human < mouse < rat, indicating the more complexity of S9 fractions than microsomes (Fig. 7B). More interesting, oral administration of AEPU at 5 mg/kg for mouse and rat, and 0.3 mg/kg for dog, resulted in a largest area under curve for dog, and then rat, while under detection limitation for mouse [37]. The species difference was also observed in other sEH inhibitors like t-AUCB, TPPU and others [31–34]. This suggests us to test the drug in corresponding species directly before we plan to employ a drug to a new species although sometimes we can draw on the experience from other species.

LC-MS/MS is a valuable analytical tool for drug metabolism [54]. The metabolites can be separated by their polarity on the LC column with the solvent gradient (Fig. 1 and 2). With different retention time of authentic standards, the metabolites with adamantyl hydroxylation (6–12 min) are separated from the metabolites with polyethylene glycol hydroxylation (12–18 min). In addition, the regioisomers of metabolites with adamantyl hydroxylation can be separated by the reverse phase chromatography employed. Because of its identical retention time, co-chromatography and mass data with the authentic standard, the second peak is a product of hydroxylation on the adamantyl group (M2). It is suggested that M1 and M6 are stereoisomers because they had same ketone products after chromic acid oxidation. The first peak is more polar suggesting *endo*-γ-hydroxylation on the adamantyl group (M1). Meanwhile, the third peak is *epi*-γ-hydroxylation (M6) due to the intra-molecular hydrogen bond leading to longer retention time. As mentioned above, this laboratory synthesized M1- and M2-like metabolites for another adamantyl-urea-based sEH inhibitor APAU. M1-like metabolite was washed out earlier than M2-like metabolite in the same column, which strongly supported the proposed structure for M1 after the structure of M2 was established.

Besides LC separation, the unique adamantyl fragmentation of mass spectrometry facilitates the identification of metabolites and increase detection sensitivity by mass spectra without using radioisotopes (Table 1). Due to the stable tertiary carbocation from electrospray ionization on the adamantyl moiety, the mass spectrum can give positive ion at *m/z* 135 to identify the metabolite with adamantyl ring [41, 55]. This property of the adamantane allows very sensitive detection of such compounds by LC-MS. The metabolites with *N*-oxidation (M3 and M4) and polyethylene glycol oxidation (M7–M14) are further confirmed by the daughter scan at *m/z* 135, even though the retention time of M3 and M4 is overlapped with

metabolites of adamantyl oxidation (M2). Furthermore, the sensitivity of adamantyl group by MS/MS facilitates detection in biological fluids [41]. Herein, only 10 μl of whole blood is needed for *in vivo* monitoring (Fig. 4) suggesting that lower doses of AEPU can be used and smaller blood samples can be collected in a clinical study.

Numerous sEH inhibitors have been published based on the first description of substituted ureas amides and carbamates by Morisseau et al [56]. Shen and Hammock have reviewed the peer reviewed and patent literatures and described possible pathways to the clinic historically [26]. AEPU was significant in showing a polar binding site in the soluble epoxide hydrolase enzyme and directing the synthetic of more drug like inhibitors[57]. The adamantane moiety is a space filling lipophilic group that leads to high activity when used in sEH inhibitors [19], but it is also used in drugs to reduce their half lives because it is rapidly metabolized [58]. Similarly polyethoxylates are rapidly metabolized and very polar. When polyethoxylates are attached to a lipophilic head a surfactant is obtained which facilitates movement into cells. Thus AEPU is a highly potent sEH inhibitor which dissolves in water easily, penetrates membranes rapidly and is rapidly metabolized systemically. This makes it ideal for ocular administration or nebulization for pulmonary inflammation. Its rapid penetration and ease of formulation in common solvents makes it a good candidate for typical treatment of pain and inflammation as in gout. In all of these indications, the high local concentrations are anticipated to drop rapidly due to metabolism as AEPU moves away from the site of local application.

In conclusion, the present studies demonstrate that AEPU metabolism in liver subcellular fractions includes adamantyl oxidation, *N*-oxidation, and polyethylene glycol oxidation. Both adamantyl moiety and polyethylene glycol chain are vulnerable for the first-pass metabolism possibly resulting from CYP 3A4. Most metabolites with oxidation on polyethylene glycol chain are metabolized *in vivo* possibly by β-oxidation to propanoic acid metabolites. The metabolism of AEPU through adamantyl oxidation and *N*-oxidation could be shared by other *N*-adamantyl substituted urea-based sEH inhibitors. The insights to this study can help future inhibitor design and further pharmacological study.

Acknowledgments

Abbreviations

AEPU	1-adamantan-1-yl-3-(5-(2-(2-ethoxyethoxy)ethoxy)pentyl)urea (also published as UC950)
t-**AUCB**	*trans*-4-[4-(3-adamantan-1-ylureido)-cyclohexyloxy]-benzoic acid
AUDA	12-(3-adamantyl-ureido)-dodecanoic acid
CDU	1-cyclohexyl-3-dodecyl-urea

CID	collision-induced dissociation
CYP	cytochrome P450
EETs	epoxyeicosatrienoic acids
LC-MS	liquid chromatography-mass chromatography
LC-MS/MS	liquid chromatography-tandem mass spectrometry
m/z	mass to charge ratio
RT	retention time
sEH	soluble epoxide hydrolase

References

1. Newman JW, Morisseau C, Hammock BD. Epoxide hydrolases: their roles and interactions with lipid metabolism. Prog Lipid Res. 2005; 44:1–51. [PubMed: 15748653]

2. Morisseau C, Hammock BD. Epoxide hydrolases: mechanisms, inhibitor designs, and biological roles. Annu Rev Pharmacol Toxicol. 2005; 45:311–33. [PubMed: 15822179]

3. Fleming I, Rueben A, Popp R, Fisslthaler B, Schrodt S, Sander A, et al. Epoxyeicosatrienoic acids regulate Trp channel dependent Ca2+ signaling and hyperpolarization in endothelial cells. Arterioscler Thromb Vasc Biol. 2007; 27:2612–8. [PubMed: 17872452]

4. Imig JD. Eicosanoids and renal damage in cardiometabolic syndrome. Expert Opin Drug Metab Toxicol. 2008; 4:165–74. [PubMed: 18248310]

5. Wang Y, Wei X, Xiao X, Hui R, Card JW, Carey MA, et al. Arachidonic acid epoxygenase metabolites stimulate endothelial cell growth and angiogenesis via mitogen-activated protein kinase and phosphatidylinositol 3-kinase/Akt signaling pathways. J Pharmacol Exp Ther. 2005; 314:522–32. [PubMed: 15840765]

6. Fleming I. Epoxyeicosatrienoic acids, cell signaling and angiogenesis. Prostaglandins Other Lipid Mediat. 2007; 82:60–7. [PubMed: 17164133]

7. Node K, Huo Y, Ruan X, Yang B, Spiecker M, Ley K, et al. Anti-inflammatory properties of cytochrome P450 epoxygenase-derived eicosanoids. Science. 1999; 285:1276–9. [PubMed: 10455056]

8. Ng VY, Huang Y, Reddy LM, Falck JR, Lin ET, Kroetz DL. Cytochrome P450 eicosanoids are activators of peroxisome proliferator-activated receptor alpha. Drug Metab Dispos. 2007; 35:1126–34. [PubMed: 17431031]

9. Chiamvimonvat N, Ho CM, Tsai HJ, Hammock BD. The soluble epoxide hydrolase as a pharmaceutical target for hypertension. J Cardiovasc Pharmacol. 2007; 50:225–37. [PubMed: 17878749]

10. Schmelzer KR, Kubala L, Newman JW, Kim IH, Eiserich JP, Hammock BD. Soluble epoxide hydrolase is a therapeutic target for acute inflammation. Proc Natl Acad Sci U S A. 2005; 102:9772–7. [PubMed: 15994227]

11. Liu JY, Yang J, Inceoglu B, Qiu H, Ulu A, Hwang SH, et al. Inhibition of soluble epoxide hydrolase enhances the anti-inflammatory effects of aspirin and 5-lipoxygenase activation protein inhibitor in a murine model. Biochem Pharmacol. 2010; 79:880–7. [PubMed: 19896470]

12. Xu D, Li N, He Y, Timofeyev V, Lu L, Tsai HJ, et al. Prevention and reversal of cardiac hypertrophy by soluble epoxide hydrolase inhibitors. Proc Natl Acad Sci U S A. 2006; 103:18733–8. [PubMed: 17130447]

13. Zhang W, Koerner IP, Noppens R, Grafe M, Tsai HJ, Morisseau C, et al. Soluble epoxide hydrolase: a novel therapeutic target in stroke. J Cereb Blood Flow Metab. 2007; 27:1931–40. [PubMed: 17440491]

14. Inceoglu B, Schmelzer KR, Morisseau C, Jinks SL, Hammock BD. Soluble epoxide hydrolase inhibition reveals novel biological functions of epoxyeicosatrienoic acids (EETs). Prostaglandins Other Lipid Mediat. 2007; 82:42–9. [PubMed: 17164131]

15. Wagner K, Inceoglu B, Dong H, Yang J, Hwang SH, Jones P, et al. Comparative efficacy of 3 soluble epoxide hydrolase inhibitors in rat neuropathic and inflammatory pain models. Eur J Pharmacol. 2013; 700:93–101. [PubMed: 23276668]

16. Hammock BD, Wagner K, Inceoglu B. The soluble epoxide hydrolase as a pharmaceutical target for pain management. Pain Manag. 2011; 1:383–6. [PubMed: 24645702]

17. Wagner K, Inceoglu B, Gill SS, Hammock BD. Epoxygenated fatty acids and soluble epoxide hydrolase inhibition: novel mediators of pain reduction. J Agric Food Chem. 2011; 59:2816–24. [PubMed: 20958046]

18. Sirish P, Li N, Liu JY, Lee KS, Hwang SH, Qiu H, et al. Unique mechanistic insights into the beneficial effects of soluble epoxide hydrolase inhibitors in the prevention of cardiac fibrosis. Proc Natl Acad Sci U S A. 2013; 110:5618–23. [PubMed: 23493561]

19. Morisseau C, Hammock BD. Impact of soluble epoxide hydrolase and epoxyeicosanoids on human health. Annu Rev Pharmacol Toxicol. 2013; 53:37–58. [PubMed: 23020295]

20. Yu G, Zeng X, Wang H, Hou Q, Tan C, Xu Q. 14,15-epoxyeicosatrienoic Acid suppresses cigarette smoke extract-induced apoptosis in lung epithelial cells by inhibiting endoplasmic reticulum stress. Cell Physiol Biochem. 2015; 36:474–86. [PubMed: 25968975]

21. Bajpai P, Srinivasan S, Ghosh J, Nagy LD, Wei S, Guengerich FP, et al. Targeting of splice variants of human cytochrome P450 2C8 (CYP2C8) to mitochondria and their role in arachidonic acid metabolism and respiratory dysfunction. J Biol Chem. 2014; 289:29614–30. [PubMed: 25160618]

22. Wang X, Ni L, Yang L, Duan Q, Chen C, Edin ML, et al. CYP2J2-derived epoxyeicosatrienoic acids suppress endoplasmic reticulum stress in heart failure. Mol Pharmacol. 2014; 85:105–15. [PubMed: 24145329]

23. Hye Khan MA, Neckar J, Manthati V, Errabelli R, Pavlov TS, Staruschenko A, et al. Orally active epoxyeicosatrienoic acid analog attenuates kidney injury in hypertensive Dahl salt-sensitive rat. Hypertension. 2013; 62:905–13. [PubMed: 23980070]

24. Khan MA, Liu J, Kumar G, Skapek SX, Falck JR, Imig JD. Novel orally active epoxyeicosatrienoic acid (EET) analogs attenuate cisplatin nephrotoxicity. Faseb J. 2013; 27:2946–56. [PubMed: 23603837]

25. Xu X, Tu L, Feng W, Ma B, Li R, Zheng C, et al. CYP2J3 gene delivery up-regulated adiponectin expression via reduced endoplasmic reticulum stress in adipocytes. Endocrinology. 2013; 154:1743–53. [PubMed: 23515292]

26. Shen HC, Hammock BD. Discovery of inhibitors of soluble epoxide hydrolase: a target with multiple potential therapeutic indications. J Med Chem. 2012; 55:1789–808. [PubMed: 22168898]

27. Hwang SH, Tsai HJ, Liu JY, Morisseau C, Hammock BD. Orally bioavailable potent soluble epoxide hydrolase inhibitors. Journal of Medicinal Chemistry. 2007; 50:3825–40. [PubMed: 17616115]

28. Lee KSS, Liu JY, Wagner KM, Pakhomova S, Dong H, Morisseau C, et al. Optimized Inhibitors of Soluble Epoxide Hydrolase Improve in Vitro Target Residence Time and in Vivo Efficacy. Journal of Medicinal Chemistry. 2014; 57:7016–30. [PubMed: 25079952]

29. Rose TE, Morisseau C, Liu JY, Inceoglu B, Jones PD, Sanborn JR, et al. 1-Aryl-3-(1-acylpiperidin-4-yl)urea inhibitors of human and murine soluble epoxide hydrolase: structure-activity relationships, pharmacokinetics, and reduction of inflammatory pain. J Med Chem. 2010; 53:7067–75. [PubMed: 20812725]

30. Kim IH, Morisseau C, Watanabe T, Hammock BD. Design, synthesis, and biological activity of 1,3-disubstituted ureas as potent inhibitors of the soluble epoxide hydrolase of increased water solubility. J Med Chem. 2004; 47:2110–22. [PubMed: 15056008]

31. Liu JY, Tsai HJ, Hwang SH, Jones PD, Morisseau C, Hammock BD. Pharmacokinetic optimization of four soluble epoxide hydrolase inhibitors for use in a murine model of inflammation. Br J Pharmacol. 2009; 156:284–96. [PubMed: 19154430]

32. Tsai HJ, Hwang SH, Morisseau C, Yang J, Jones PD, Kasagami T, et al. Pharmacokinetic screening of soluble epoxide hydrolase inhibitors in dogs. Eur J Pharm Sci. 2010; 40:222–38. [PubMed: 20359531]

33. Ulu A, Appt S, Morisseau C, Hwang SH, Jones PD, Rose TE, et al. Pharmacokinetics and in vivo potency of soluble epoxide hydrolase inhibitors in cynomolgus monkeys. Br J Pharmacol. 2012; 165:1401–12. [PubMed: 21880036]

34. Liu JY, Lin YP, Qiu H, Morisseau C, Rose TE, Hwang SH, et al. Substituted phenyl groups improve the pharmacokinetic profile and anti-inflammatory effect of urea-based soluble epoxide hydrolase inhibitors in murine models. Eur J Pharm Sci. 2013; 48:619–27. [PubMed: 23291046]

35. Guedes AG, Morisseau C, Sole A, Soares JH, Ulu A, Dong H, et al. Use of a soluble epoxide hydrolase inhibitor as an adjunctive analgesic in a horse with laminitis. Vet Anaesth Analg. 2013; 40:440–8. [PubMed: 23463912]

36. Watanabe T, Morisseau C, Newman JW, Hammock BD. In vitro metabolism of the mammalian soluble epoxide hydrolase inhibitor, 1-cyclohexyl-3-dodecyl-urea. Drug Metab Dispos. 2003; 31:846–53. [PubMed: 12814960]

37. Kim IH, Tsai HJ, Nishi K, Kasagami T, Morisseau C, Hammock BD. 1,3-disubstituted ureas functionalized with ether groups are potent inhibitors of the soluble epoxide hydrolase with improved pharmacokinetic properties. J Med Chem. 2007; 50:5217–26. [PubMed: 17894481]

38. Watanabe T, Hammock BD. Rapid determination of soluble epoxide hydrolase inhibitors in rat hepatic microsomes by high-performance liquid chromatography with electrospray tandem mass spectrometry. Anal Biochem. 2001; 299:227–34. [PubMed: 11730347]

39. Jones PD, Wolf NM, Morisseau C, Whetstone P, Hock B, Hammock BD. Fluorescent substrates for soluble epoxide hydrolase and application to inhibition studies. Anal Biochem. 2005; 343:66–75. [PubMed: 15963942]

40. Ulu A, Davis BB, Tsai HJ, Kim IH, Morisseau C, Inceoglu B, et al. Soluble epoxide hydrolase inhibitors reduce the development of atherosclerosis in apolipoprotein e-knockout mouse model. J Cardiovasc Pharmacol. 2008; 52:314–23. [PubMed: 18791465]

41. Watanabe T, Schulz D, Morisseau C, Hammock BD. High-throughput pharmacokinetic method: Cassette dosing in mice associated with minuscule serial bleedings and LC/MS/MS analysis. Anal Chim Acta. 2006; 559:37–44. [PubMed: 16636700]

42. Loh AC, Szuna AJ, Williams TH, Sasso GJ, Leinweber FJ. The metabolism of [14C]rimantadine hydrochloride in rats and dogs. Drug Metab Dispos. 1991; 19:381–7. [PubMed: 1676641]

43. Chaudhary KR, Abukhashim M, Hwang SH, Hammock BD, Seubert JM. Inhibition of soluble epoxide hydrolase by trans-4- [4-(3-adamantan-1-yl-ureido)-cyclohexyloxy]-benzoic acid is protective against ischemia-reperfusion injury. J Cardiovasc Pharmacol. 2010; 55:67–73. [PubMed: 19834332]

44. Iyer A, Kauter K, Alam MA, Hwang SH, Morisseau C, Hammock BD, et al. Pharmacological inhibition of soluble epoxide hydrolase ameliorates diet-induced metabolic syndrome in rats. Exp Diabetes Res. 2012; 2012:758614. [PubMed: 22007192]

45. Shaik JS, Ahmad M, Li W, Rose ME, Foley LM, Hitchens TK, et al. Soluble epoxide hydrolase inhibitor trans-4-[4-(3-adamantan-1-yl-ureido)-cyclohexyloxy]-benzoic acid is neuroprotective in rat model of ischemic stroke. Am J Physiol Heart Circ Physiol. 2013; 305:H1605–13. [PubMed: 24043255]

46. Shen L, Peng H, Zhao S, Xu D. A potent soluble epoxide hydrolase inhibitor, t-AUCB, modulates cholesterol balance and oxidized low density lipoprotein metabolism in adipocytes in vitro. Biol Chem. 2014; 395:443–51. [PubMed: 24225128]

47. Jia L, Liu X. The conduct of drug metabolism studies considered good practice (II): in vitro experiments. Curr Drug Metab. 2007; 8:822–9. [PubMed: 18220563]

48. Brandon EF, Raap CD, Meijerman I, Beijnen JH, Schellens JH. An update on in vitro test methods in human hepatic drug biotransformation research: pros and cons. Toxicol Appl Pharmacol. 2003; 189:233–46. [PubMed: 12791308]

49. He H, Tran P, Yin H, Smith H, Flood D, Kramp R, et al. Disposition of vildagliptin, a novel dipeptidyl peptidase 4 inhibitor, in rats and dogs. Drug Metab Dispos. 2009; 37:545–54. [PubMed: 19074976]

50. Morisseau C, Goodrow MH, Newman JW, Wheelock CE, Dowdy DL, Hammock BD. Structural refinement of inhibitors of urea-based soluble epoxide hydrolases. Biochem Pharmacol. 2002; 63:1599–608. [PubMed: 12007563]

51. Hwang SH, Morisseau C, Do Z, Hammock BD. Solid-phase combinatorial approach for the optimization of soluble epoxide hydrolase inhibitors. Bioorg Med Chem Lett. 2006; 16:5773–7. [PubMed: 16949285]

52. Fink-Gremmels J. Implications of hepatic cytochrome P450-related biotransformation processes in veterinary sciences. Eur J Pharmacol. 2008; 585:502–9. [PubMed: 18417118]

53. Jia L, Noker PE, Coward L, Gorman GS, Protopopova M, Tomaszewski JE. Interspecies pharmacokinetics and in vitro metabolism of SQ109. Br J Pharmacol. 2006; 147:476–85. [PubMed: 16432511]

54. Youdim KA, Saunders KC. A review of LC-MS techniques and high-throughput approaches used to investigate drug metabolism by cytochrome P450s. J Chromatogr B Analyt Technol Biomed Life Sci.

55. Almeida AA, Campos DR, Bernasconi G, Calafatti S, Barros FAP, Eberlin MN, et al. Determination of memantine in human plasma by liquid chromatography-electrospray tandem mass spectrometry: Application to a bioequivalence study. Journal of Chromatography B. 2007; 848:311–6.

56. Morisseau C, Goodrow MH, Dowdy D, Zheng J, Greene JF, Sanborn JR, et al. Potent urea and carbamate inhibitors of soluble epoxide hydrolases. Proc Natl Acad Sci U S A. 1999; 96:8849–54. [PubMed: 10430859]

57. Jones PD, Tsai HJ, Do ZN, Morisseau C, Hammock BD. Synthesis and SAR of conformationally restricted inhibitors of soluble epoxide hydrolase. Bioorg Med Chem Lett. 2006; 16:5212–6. [PubMed: 16870439]

58. Lamoureux G, Artavia G. Use of the adamantane structure in medicinal chemistry. Curr Med Chem. 2010; 17:2967–78. [PubMed: 20858176]
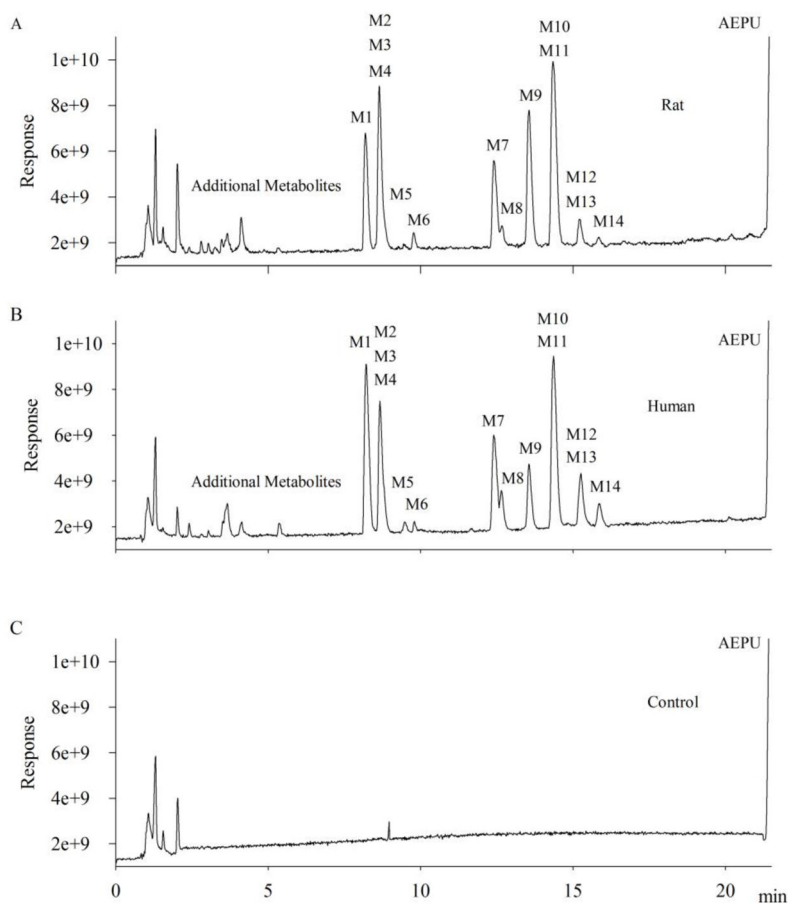
Fig. 1.
Chromatograms of AEPU incubated within 60 minutes in rat (A) and human (B) liver S9
fraction by LC/MS. Note that M2 and AEPU were identified by retention times and CID
product ion spectra that were identical to those of their synthetic standards, whereas the
other metabolite structures were assigned based on the mass spectrometric data and NMR
spectra. Metabolites structures were tentatively assigned based on both identical retention
time and co-chromatogrphy with authentic synthetic standards and metabolites generated
with S9 incubations.
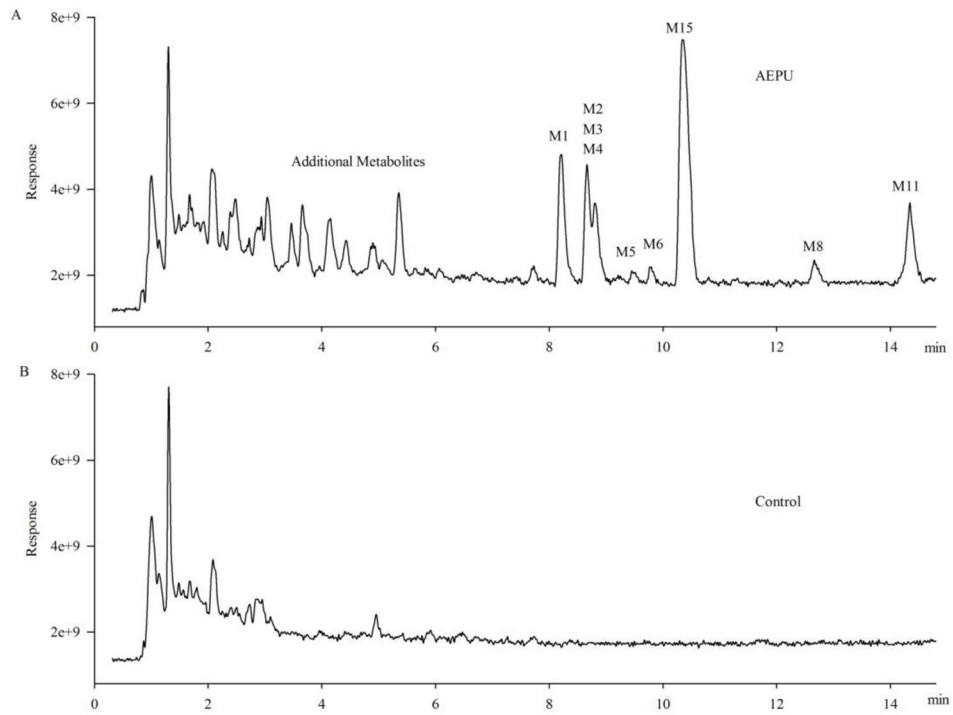
Fig. 2.
Chromatograms of AEPU metabolites in rat urine. The metabolite IDs are identical to those in Fig.1.
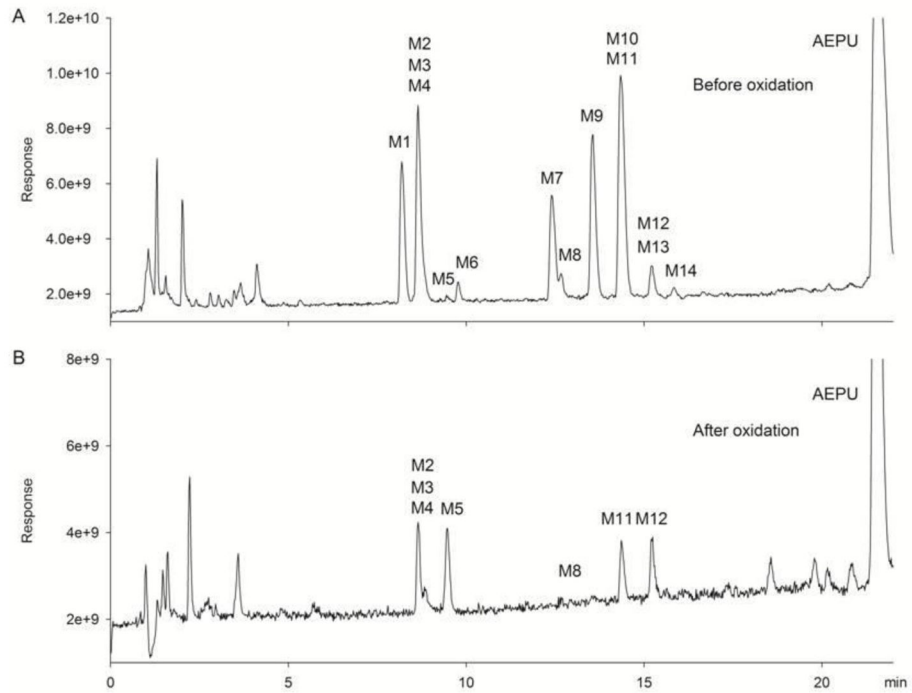
Fig. 3.
Chromatograms of AEPU hydroxylated metabolites in rat liver S9 fraction before (A) and after (B) chromic acid oxidation. M2 keep unchanged while M1 and M6 were oxidized by chromic acid, resulting in an increase in M5. In addition, M7, M9, M10, M13 and M14 were also oxidized by chromic acid.
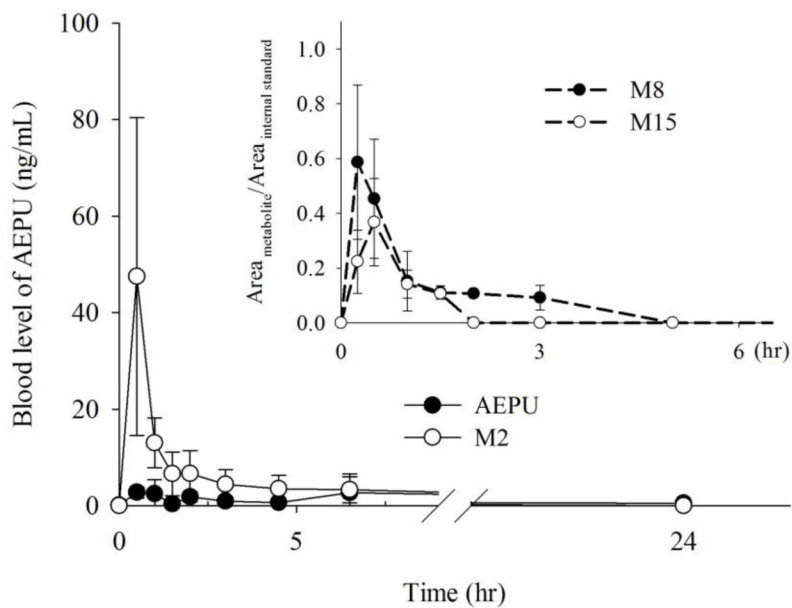
Fig. 4.
Blood level-time course of AEPU and its adamantyl hydroxylation metabolites with an oral dose of 10 mg/kg in male swiss webster mice (n = 4). Insert: Blood level-time course of the other two metabolites. Due to the lack of standards, the metabolites were semi-quantified by the ratio of response area of metabolites to the response area of internal standard on the chromatograms.
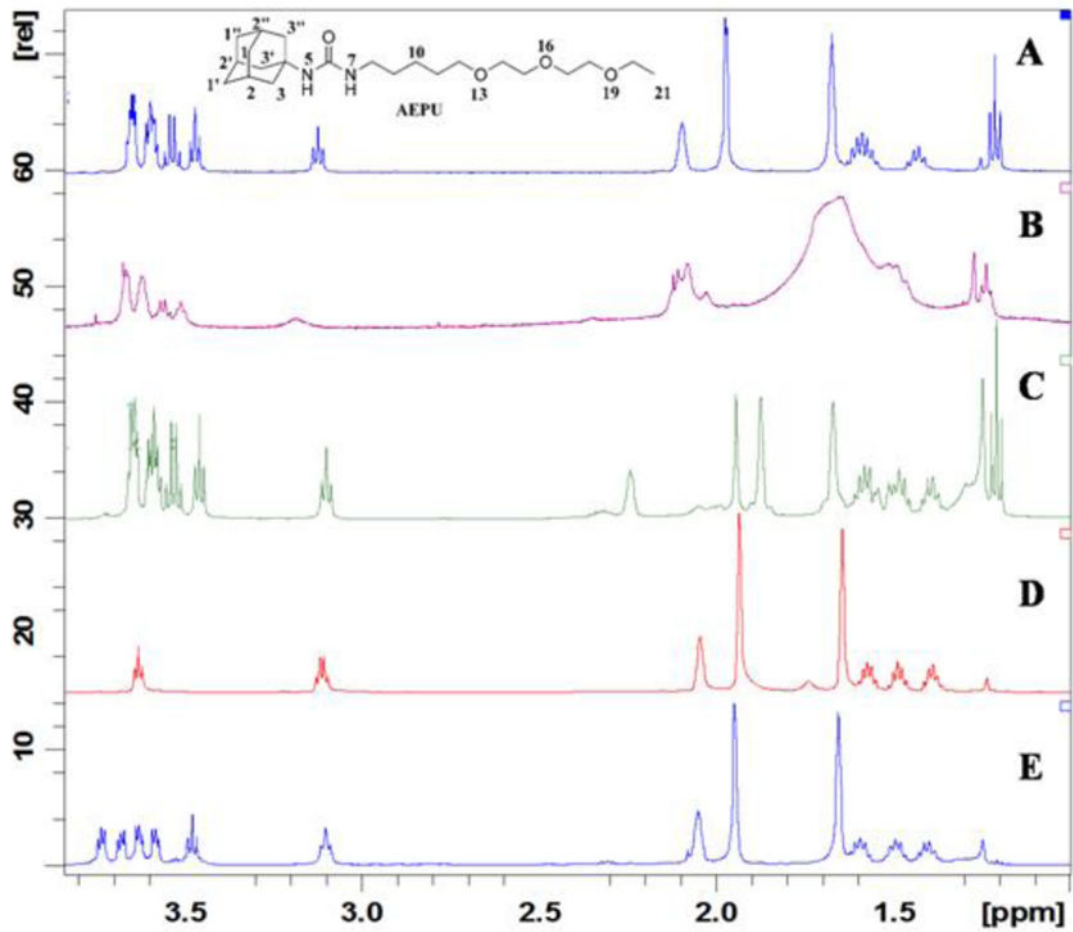
Fig. 5.
^{1}H-NMR spectra of AEPU (A) and its metabolites M1 (B), M2 (C), M7 (D) and M10 (E) collected on a Bruker Avance 500 spectrometer with ^{1}H observed at 500 MHz in CDCl_3.
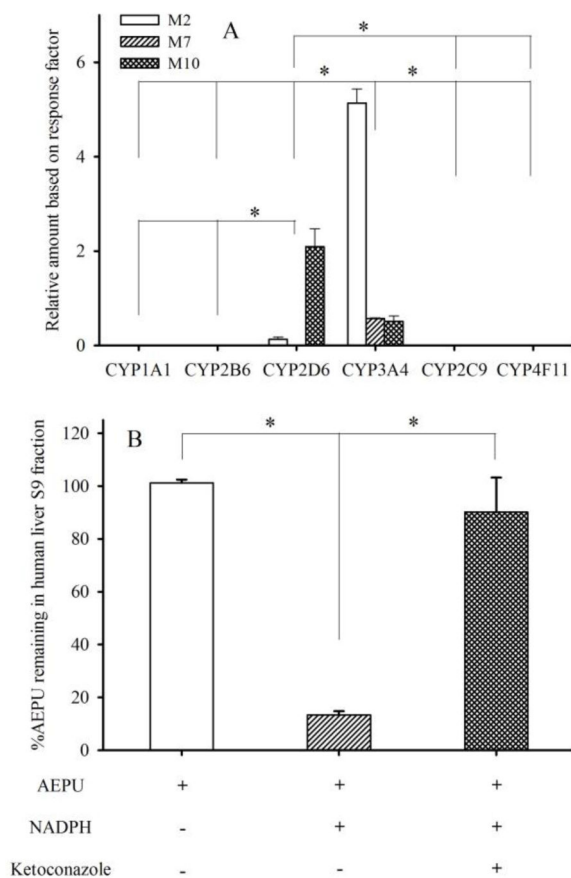
Fig. 6.
Identification of CYPs for metabolizing AEPU. (A) CYP 2D6 and 3A4 were major enzymes to metabolize AEPU. The metabolites were compared by the ratio of response are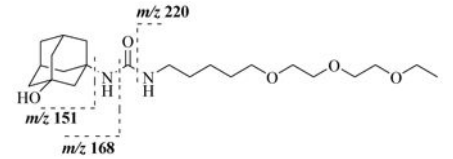a of metabolite to the response area of internal standard on the chromatograms. The appearance of metabolites following incubation with different P450s is consistent with the decrease in AEPU starting material in the incubation. (B) In human S9 fractions, AEPU metabolism was inhibited by ketoconazole, a well-known CYP 3A4 inhibitor. Data represent mean ± sd (N = 4). * (P<0.001) indicates significant difference between groups determined by ANOVA following Games-Howell analysis. M7 from CYP2D6 was of the same level as those from CYP1A1, CYP2B6, CYP2C9, and CYP4F11.
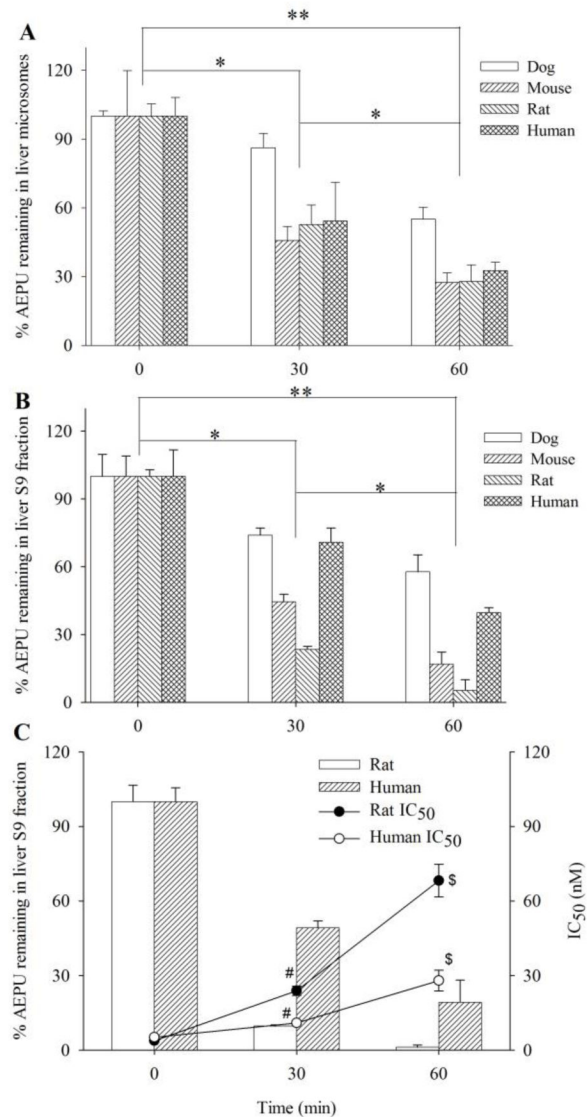
Fig. 7.
Time course of *in vitro* metabolism of AEPU in dog, mouse, rat, and human liver microsomal (A) and S9 fraction (B). (C) Time course of *in vitro* metabolism of AEPU in rat and human liver S-9 fraction and the corresponding *in vitro* inhibitory action of the metabolite mixture determined with fluorescent assay and respective recombinant purified enzymes after removal of the AEPU starting material by chromatographic approaches for 30 and 60 min while the IC_{50} data at 0 min represent the data for AEPU. Data represent mean ± sd (N = 4). In (A) and (B), * ($P<0.01$) and **($P<0.001$) indicate significant difference between groups determined by ANOVA following Turkey's or Games-Howell analysis. In (C), # ($P<0.05$) indicates significantly different from time 0 and 60 min while \$ ($P<0.01$) indicates significantly different from time 0 determined by ANOVA following Turkey's or Games-Howell analysis.
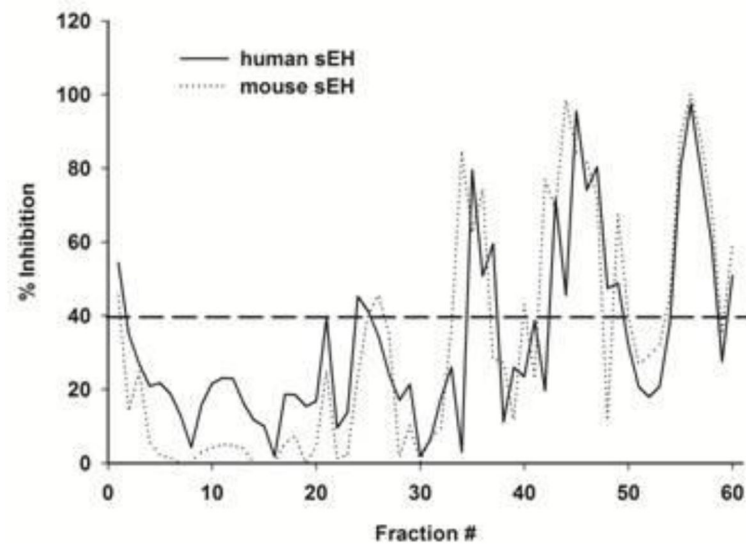
Fig. 8.
In vitro inhibition of fractions from AEPU metabolite mixture. The inhibition percentage was normalized with AEPU IC$_{50}$.
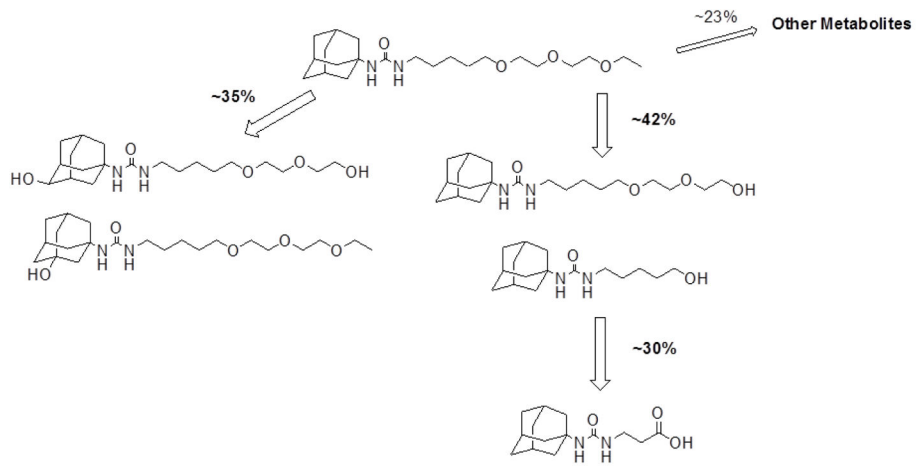
Fig. 9.
The scheme of the metabolism of AEPU. The percentage was calculated based on the ratios of response area of metabolites to the response of internal standard.
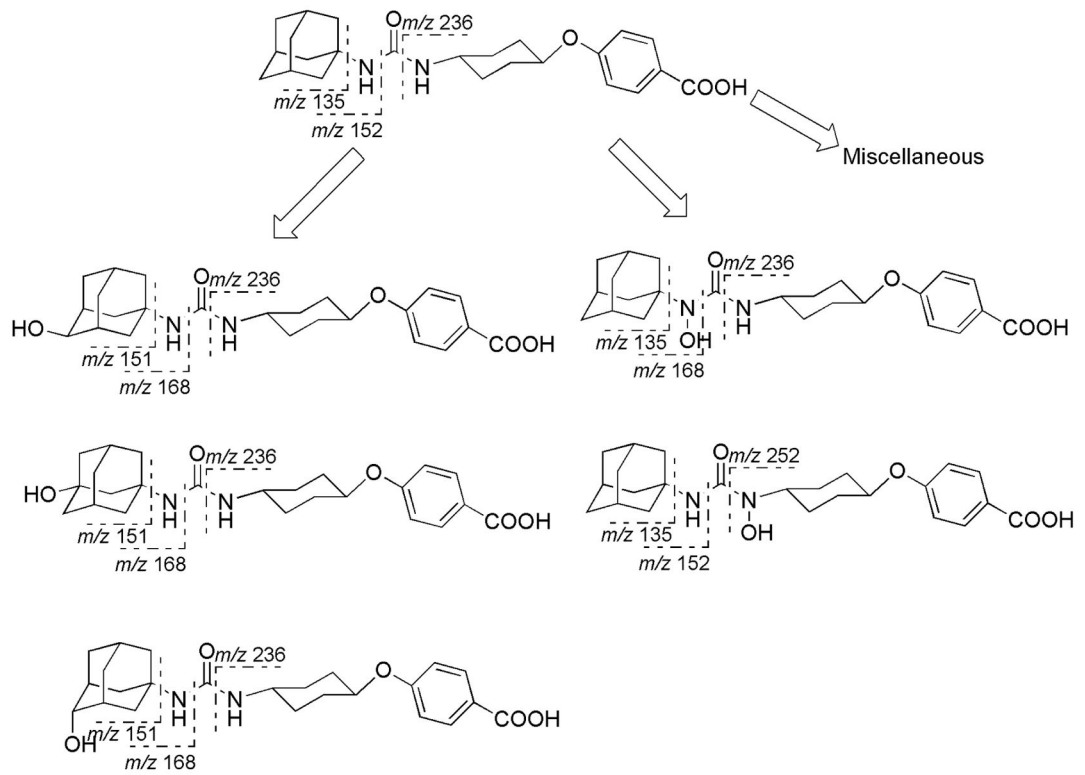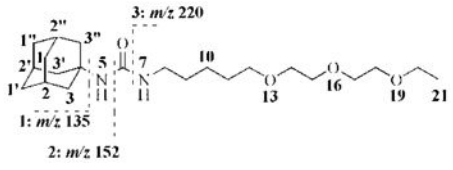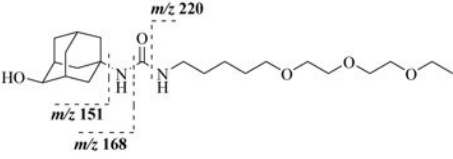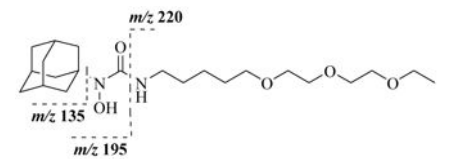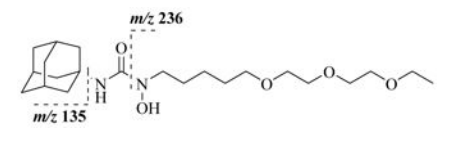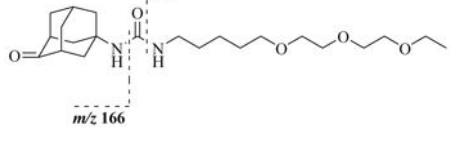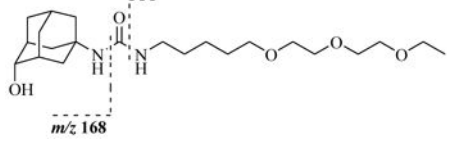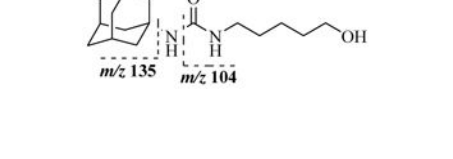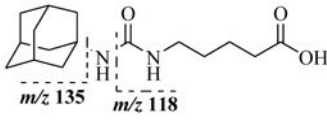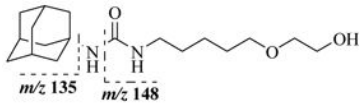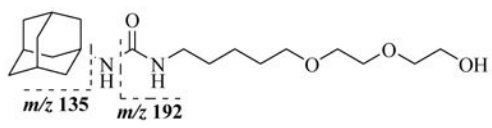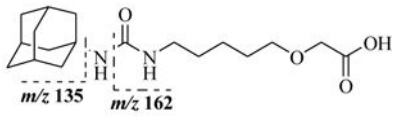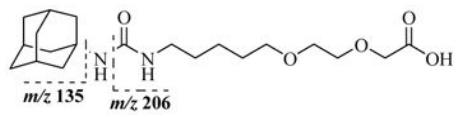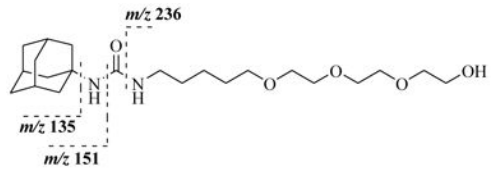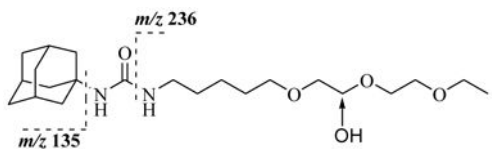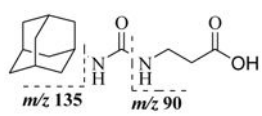
Fig. 10.
A putative scheme of the metabolism of *t*-AUCB.

Table 1

Putative structure of metabolites of AEPU identified by LC-MS/MS

Met. ID[*]	Retention time (min)	[M+H]$^+$ (m/z)	Key fragments (m/z)	Proposed structure[#]
AEPU	21.5	397	135, 152, 220	
M1	8.2	413	151, 168, 220	
M2	8.6	413	151, 168, 220	
M3	8.8	413	135, 220,195	
M4	8.8	413	135, 236	
M5	9.5	411	166, 220	
M6	9.8	413	151, 220	
M7	12.4	281	104, 135	

Biochem Pharmacol. Author manuscript; available in PMC 2016 December 15.

Met. ID[*]	Retention time (min)	[M+H]+ (m/z)	Key fragments (m/z)	Proposed structure[#]
M8	12.6	295	118, 135	
M9	13.5	325	135, 148	
M10	14.3	369	135, 192	
M11	14.3	339	135, 162	
M12	15.2	383	135, 206	
M13	15.2	413	135, 151, 236	
M14[*]	15.8	413	135, 236	
M15	10.3	267	90, 135	

Metabolite IDs were identical to those in Fig. 1 and 2.

[*] The tentative structure of M14 needs further study.

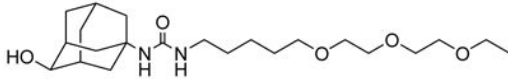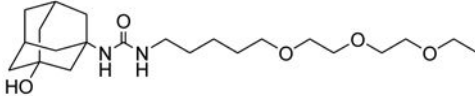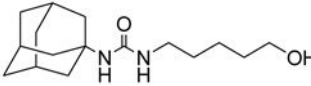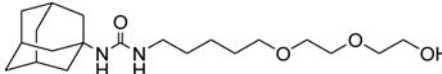[#] Some fragments involve in the shift and rearrangement of protons.
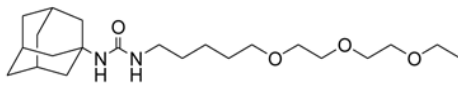
Table 2

¹H-NMR analysis of AEPU and its key metabolites

Position	AEPU	M1	M2	M7	M10
1	1.67 (2H, br s)	3.94 (1H, br d)	1.67(2H, br s)	1.64 (2H, br s)	1.62 (2H, br s)
1′	1.67 (2H, br s)	ND*	1.67 (2H, br s)	1.64 (2H, br s)	1.62 (2H, br s)
1″	1.67 (2H, br s)	ND	1.48 (2H, br s)	1.64 (2H, br s)	1.62 (2H, br s)
2	2.09 (1H, br s)	ND	-	2.04 (1H, br s)	2.08 (1H, br s)
2′	2.09 (1H, br s)	ND	2.24 (1H, br s)	2.04 (1H, br s)	2.08 (1H, br s)
2″	2.09 (1H, br s)	ND	2.24 (1H, br s)	2.04 (1H, br s)	2.08 (1H, br s)
3	1.97 (2H, br d, 2.5)	ND	1.94 (2H, br s)	1.93 (2H, br d, 2.5)	1.87 (2H, br d, 2.5)
3′	1.97 (2H, br d, 2.5)	ND	1.84 (2H, br s)	1.93 (2H, br d, 2.5)	1.87 (2H, br d, 2.5)
3″	1.97 (2H, br d, 2.5)	ND	1.84(2H, br s)	1.93 (2H, br d, 2.5)	1.87 (2H, br d, 2.5)
8	3.12 (2H, t, 7.0)	3.18 (2H, t, 6.5)	3.10 (2H, t, 6.6)	3.11 (2H, dd 10.6, 5.5)	3.10 (2H, t, 6.0)
9	1.58 (2H, m)	ND		1.49 (2H, m)	1.48 (2H, m)
10	1.41 (2H, m)	ND	1.37 (2H, m)	1.39 (2H, m)	1.39 (2H, m)
11	1.58 (2H, m)	ND		1.57 (2H, m)	1.59 (2H, m)
12	3.46 (2H, t, 6.2)	3.51 (2H, t, 6.0)	3.46 (2H, t, 6.3)	3.63 (2H, t, 6.4)	3.46 (2H, t, 5.5)
14	3.59 (2H, m)	3.62 (2H, m)	3.57 (2H, m)	-	3.58 (2H, m)
15	3.59 (2H, m)	3.62 (2H, m)	3.57 (2H, m)	-	3.68 (2H, m)
17	3.65 (2H, m)	3.66 (2H, m)	3.64 (2H, m)	-	3.62 (2H, br t, 5.0)
18	3.65 (2H, m)	3.66 (2H, m)	3.64 (2H, m)	-	3.73 (2H, br t, 5.0)
20	3.53 (2H, q, 7.0)	3.57 (2H, q, 6.6)	3.53 (2H, q, 6.0)	-	-
21	1.21 (3H, t, 7.0)	1.24 (3H, t, 6.6)	1.20 (3H, t, 6.0)	-	-

*
ND means not design because heavily overlap. Compounds were dissolved in CDCl3 for NMR data collection on a Bruker Avance 500 spectrometer with ¹H observed at 500 MHz. The chemical shifts were expressed in δ (ppm) relative to SiMe4 (the internal standard) with coupling constants J in Hz

Table 3

IC$_{50}$ of AEPU metabolites determined by *in vitro* fluorescent assay

Met. ID.	Structure	IC$_{50}$ (nM)	
		Human sEH	Mouse sEH
M1		480	290
M2		870	80
M7		84	5
M10		15	6
AEPU		14	3